

# On the Invariance of Residues of Feynman Graphs

Isabella Bierenbaum\*, Richard Kreckel†

Department of Physics, Mainz University, D-55099 Mainz, Germany

Dirk Kreimer‡

Mathematics Department, Boston University, Boston MA02215, USA

November 21, 2001

## Abstract

We use simple iterated one-loop graphs in massless Yukawa theory and QED to pose the following question: what are the symmetries of the residues of a graph under a permutation of places to insert subdivergences. The investigation confirms partial invariance of the residue under such permutations: the highest weight transcendental is invariant under such a permutation. For QED this result is gauge invariant, i.e. the permutation invariance holds for any gauge. Computations are done making use of the Hopf algebra structure of graphs and employing GiNaC to automate the calculations.

## 1 Introduction

This paper serves three purposes: i) it employs GiNaC [1] in Feynman diagram calculations and provides algorithms which automate the renormalization process, very much in the spirit of [2]; ii) it investigates symmetries of short distance singularities under permutations of places where to insert subdivergences in a graph; iii) it once more confirms the presence or absence of transcendental coefficients of short-distance singularity in accordance with the topology of a graph.

Our laboratory of investigation are simple one-loop Feynman graphs in massless Yukawa theory or QED, inserted into each other in tree-like hierarchies. Thus, the combinatorics of renormalization boils down to the Hopf algebra of decorated rooted trees with only a small number of decorations and the analytical challenge posed by those decorations reduces to expansions of  $\Gamma$ -functions near unit argument. The question we can ask is for the distribution of the Riemann  $\zeta$ -function over the various poles in the Laurent series of graphs of that form.

In contrast to [2] and subsequent papers [3], where the renormalization problem was automated in a similar context optimized for speed and efficiency, we have developed here algorithms which allow for non-trivial spin-structures and an easy generalization to arbitrary decorations: the primitive decorations can be inserted as arguments so that the algorithm can handle arbitrary primitive graphs when their analytic structure becomes known.

We work in the context of dimensional regularization, so that any Feynman graph becomes a Laurent series in  $\epsilon = (4 - D)/2$ , the deviation of the dimension from its integer value four, and the pole terms reflect the short distance singularities in the theory. The first order pole is

---

\*e-mail: bierenbaum@thep.physik.uni-mainz.de

†e-mail: richard.kreckel@uni-mainz.de

‡e-mail: dkreimer@bu.edu

denoted as the residue of a graph. Its significance lies in the fact that higher pole terms can be reduced to polynomials in residues [4], and in the fact that the residue of a primitive graph is an invariant under diffeomorphisms of external parameters of the graph (diffeomorphisms of external momenta and masses) as well as an invariant under variations of renormalization schemes. Such a residue is a motivic number then in some modern mathematic parlance. The question as to which class of such numbers is sufficient to describe the residues of a given quantum field theory is open and fascinating [5].

We only study two much more basic questions, motivated by previous and ongoing investigations into the analytic structure of pole terms and residues in particular.

The first is the independence of the appearance of transcendentals under variations of the quantum field theory which realizes a graph with a given topology. To specify the topology of a one-particle irreducible Feynman graph  $\Gamma$ , let us consider the adjacency matrix  $M(\Gamma)$  of  $\Gamma$ . If  $\Gamma$  has  $n$  vertices, this matrix is a  $n \times n$  matrix. We take for its non-zero entries pairs (propagator type, powercounting weight), ie. each non-zero entry  $M(\Gamma)_{ij}$  specifies that vertex  $i$  is connected to vertex  $j$  by a propagator of some type, which has a certain powercounting weight.<sup>1</sup> In the cases studied here, the possible entries are

$$(\text{fermion},1),(\text{photon},2),(\text{scalar boson},2).$$

The listing of the powercounting weight is redundant, as it is determined by the type of the propagator. We list it just for easy reference.

The graphs of QED and Yukawa theory which we will compare always have adjacency matrices which agree in all their zero entries,

$$M(\Gamma_{\text{QED}})_{ij} = 0 \Leftrightarrow M(\Gamma_{\text{Yuk}})_{ij} = 0$$

and agree for each non-zero entry in the powercounting degree of the corresponding edge. It is only the nature of the edges which changes from the spin one vector boson propagator –the QED photon– to the spin zero scalar boson propagator in Yukawa theory. Note that the structure of short distance singularity then remains fixed in the transition of one theory to the other. We then expect and confirm that rational numbers can vary in the transition from one theory to the other, while the transcendentals we see remain invariant and specific for the chosen topology. Here, a topology is uniquely described by considering in such an adjacency matrix all non-zero entries as equal. So it just gives information about how vertices are connected, but forgets about the nature of the propagators establishing that connection. To find non-rational numbers, we have to go up to four loops at least in the simple class of Feynman graphs which we consider. There, it is the swiss cheese topology of Fig.1a in which we expect to see a residue  $\sim \zeta(3)$ , while the ladder topology of Fig.1b are known to have only rational residues [6].

The second question is of different nature: for a log-divergent vertex graph which is primitive under the coproduct, it is evident that its residue has the above mentioned invariances. The Hopf algebra structure immediately allows to prove that in a vertex graph which is not primitive under the coproduct such that the graph contains divergent subgraphs, the coefficient of the highest order pole still has these symmetries and is given by an easy calculable product of residues with a combinatorial factor, determined by the scattering type formula of [4], which incorporates the 't Hooft relations between higher pole terms in graphs.

---

<sup>1</sup>We can notate the type of vertex in the diagonal entries of this symmetric matrix (no vertex is connected to itself by a propagator).

What we call here the 't Hooft relations in accordance with [4] is the simple fact that higher order poles in a graph  $\Gamma$  with UV-divergent subgraphs  $\gamma$  can be calculated from products of lower order poles of these subgraphs  $\gamma$  and their complements  $\Gamma/\gamma$ . This is well-known and a necessary requirement to make the renormalization group work: the  $Z$ -factor for a given physical quantity is an invertible (it starts with 1) formal series over counterterms of graphs such that its logarithmic derivative with respect to the variation of the renormalization scale  $\nu$ ,  $d\log(Z)/d\nu^2$ , is finite. This finiteness establishes relations between pole terms which, for the case of dimensional regularization, were, it seems, first explored by 't Hooft. These relations are a direct consequence of the mathematical structure of the Hopf algebra underlying renormalization, and its one-parameter group of automorphisms [4].

Let us now consider the residue of such a graph which does have divergent subgraphs. Typically, this residue will be a number which can be decomposed in terms of transcendental weight: it will contain contributions ranging from rational numbers to monomials in  $\zeta(j)$  of up to transcendental weight  $l - 1$ , where  $l$  is the bidegree of the graph, calculated from its coproduct [7]<sup>2</sup>. We cannot expect the whole residue to be invariant under the above symmetries, as rational numbers can and will vary freely. But here we report a remarkable partial symmetry observed in our rather restricted lab of iterated one-loop graphs: the highest weight transcendental in the residue is invariant under permutations of external momentum as described below. We confirm this by empirical calculation to high loop orders. We finally prove the result in the context of the simple iterated one-loop graphs considered here. One has an almost elementary proof in this context and we will discuss the difficulties which arise in the general case. The nature of this result fits nicely with a structural investigation of Dyson-Schwinger equations to be delivered elsewhere [8]. Note again that changing the momentum flow but maintaining the topology corresponds to alterations of the type of non-zero entries in a suitable adjacency matrix, as Fig.2 clearly exhibits. Again, the degree of powercounting and hence the structure of short distance singularities, as well as the topology, remain unchanged.

To understand the type of symmetry we want to investigate, let us consider the one-loop vertex function. If  $\Gamma(p_1, p_2, p_3)$  is a vertex correction with momentum  $p_1$  for the external boson,  $p_2$  for the incoming fermion and  $p_3 = p_1 + p_2$  for the outgoing fermion, then we will compare  $\Gamma^1 := \Gamma(0, p, p)$  with  $\Gamma^2 := \Gamma(p, p, 0)$  at the one-loop level. It is a single permutation of the flow of an external momentum for a vertex function at zero momentum transfer, which distinguishes the two one-loop functions. Locality of counterterms ensures that the counterterm for a vertex correction graph is invariant under this permutation for any graph. So nothing exciting can be learned from just changing the momentum flow in a given vertex graph. Now let us start with such one-loop vertex corrections and let us insert more one-loop vertex corrections always at the vertex of zero momentum transfer (zmt), which indeed changes under the above permutation. This gives the topological equivalent Feynman graphs  $\Gamma^1, \Gamma^2$ , with permuted types of propagators, of Fig.2. They indeed have adjacency matrices such that again

$$M(\Gamma^1)_{ij} = 0 \Leftrightarrow M(\Gamma^2)_{ij} = 0.$$

Note that it is the requirement to maintain the same topology which forces us to consider quite different looking graphs. For them, the usual field theoretic requirements only demand that the coefficients of the highest order poles are identical. All non-leading pole terms in  $\epsilon$  do not have to and indeed do not agree.

---

<sup>2</sup>For all graphs considered here, it simply agrees with the number of loops in Yukawa theory. For the QED vertex, a shift by one unit can appear as explained later in the text.

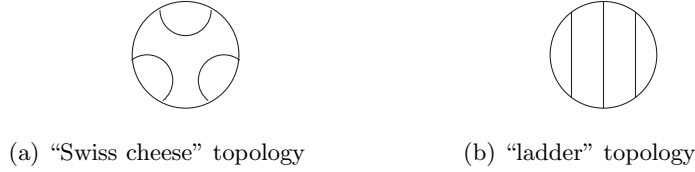


Figure 1: “Swiss cheese” and “ladder” master topology.

But a closer investigation will establish a remaining partial symmetry between those graphs, such that the highest weight transcendental in the residue is invariant. Such symmetries are of great interest. Feynman graphs with subdivergences can be built by using the pre-Lie structure of graphs, which results from underlying insertion operads [5]. The question to what extent the permutation group acts trivially under such insertions is a natural question in operad theory which needs to be answered to understand these operads. It directly leads to the questions studied here in a simplified context. We regard the results reported here as a first step in a detailed analysis of actions of the permutation group in this context.

With regard to the first question, we remind the reader that for a massless Yukawa theory represented as a Laurent-series in  $\varepsilon$ , it was already shown in [9] that graphs with the swiss cheese topology of figure 1.a possess a  $\zeta(n)$  in their counterterm, whereas graphs with a ladder topology like in figure 1.b just evaluate to rational coefficients. Similar results were obtained in QED and other theories for vertex functions of type  $\Gamma(0, p, p)$  and self-energies, in [2, 3, 6].

Our first aim is now to find out if this remains true in massless QED for both types of momentum flow and if there are any symmetries in the coefficients of the  $\zeta$ -functions in both theories, under the permutation between the two types of vertex functions  $\Gamma^1$  and  $\Gamma^2$ . Therefore we will rebuild the scheme given in [9] for the massless Yukawa theory with an extension to vertex corrections that carry a different flow of momentum in the sense described above, and similarly for QED using the matrix calculus of [10]. The resulting algorithm is implemented using the GiNaC library and will be described in section 5. With the help of this program, we will calculate the antipode of graphs that represent the different topologies given above and compare them.

## 2 Calculations

Consider a one-loop contribution to the fermionic propagator:

$$\equiv \Sigma_{[0,0]}(q^2) = \int d^D k \frac{1}{(\not{q} + \not{k})} \frac{1}{k^2}$$

where the subscript “[0, 0]” will soon serve to give the number of one-loop subdivergences to be inserted inside the diagram at the fermionic or bosonic line. All integrals considered in

this paper can be reduced to integrals  $F_{a,b}$  [11]:<sup>3</sup>

$$\begin{aligned} I(q; a, b) &\equiv \frac{1}{(\nu^2)^{-\varepsilon}} \int d^D k \frac{1}{[k^2]^a [(q-k)^2]^b} \\ &=: \frac{1}{(\nu^2)^{-\varepsilon}} [q^2]^{(2-(a+b)-\varepsilon)} F_{a,b} \end{aligned} \quad (1)$$

with

$$F_{a,b} \equiv F_{b,a} := \frac{\Gamma(2-a-\varepsilon) \Gamma(2-b-\varepsilon) \Gamma(a+b-2+\varepsilon)}{\Gamma(a) \Gamma(b) \Gamma(4-a-b-2\varepsilon)}, \quad (2)$$

which we typically need for  $a = n_1 + n_2\varepsilon, b = m_1 + m_2\varepsilon$ , for integers  $n_1, n_2, m_1, m_2$ . This reduces the identification of non-rationals (transcendentals, we dare say in the following) to an expansion of the  $\Gamma$ -function near unit argument, as promised. Note that

$$F_{a,-n} = F_{-n,b} = 0 \quad , \quad n \in \mathbb{N}^0. \quad (3)$$

Accordingly, in our conventions

$$\Sigma_{[0,0]}(q^2) = [q^2]^{-\varepsilon} \frac{1}{2} F_{1,1} \not\equiv [q^2]^{-\varepsilon} \Sigma_{0,0} \not\equiv. \quad (4)$$

## 2.1 Yukawa theory

The study of iterated one-loop integrals reduces to the study of the following elementary functions, which we will call *characterizing functions*: The one-loop fermion self-energy with insertions at its two internal propagators demands knowledge of

$$\Sigma_{i,j} := \frac{1}{2} [F_{i\varepsilon,1+j\varepsilon} + F_{1+i\varepsilon,1+j\varepsilon} - F_{1+i\varepsilon,j\varepsilon}]. \quad (5)$$

The one-loop boson self-energy with insertions at its two internal edges is given by  $\Pi_{i,j}$  and the two one-loop vertex functions at zero momentum transfer with insertions at either the zero momentum vertex, or internal lines, need knowledge of functions  $\Gamma_{i,j}$  for the vertex corrections.

$$\Pi_{i,j} / [\text{tr}(\mathbf{1})] := -\frac{1}{2} [F_{i\varepsilon,1+j\varepsilon} - F_{1+i\varepsilon,1+j\varepsilon} + F_{1+i\varepsilon,j\varepsilon}] \quad (6)$$

$$\Gamma_{i,j}^1 := F_{1+i\varepsilon,1+j\varepsilon} \quad (7)$$

$$\Gamma_{i,j}^2 := \frac{1}{2} [F_{2+i\varepsilon,j\varepsilon} - F_{2+i\varepsilon,1+j\varepsilon} + F_{1+i\varepsilon,1+j\varepsilon}]. \quad (8)$$

Here, we have divided the boson self-energy by the trace of the unit matrix  $\text{tr}(\mathbf{1})$  (trace over spinorial indices) for easier comparison of insertions of subgraphs into bosonic and fermionic lines.

---

<sup>3</sup>These  $\Gamma$ -functions will give rise to the  $\zeta$ -functions we are looking for. An easy way to see the connection between the  $\Gamma$ - and the  $\zeta$ -function is the formula:

$$\Gamma(1+\varepsilon) = \exp(-\gamma\varepsilon) \exp\left(\sum_{n=2}^{\infty} \frac{\zeta(n)}{n} (-\varepsilon)^n\right), \quad |\varepsilon| < 1$$

Internally, GiNaC follows a different approach. It computes the derivatives  $\Gamma'(x) = \Gamma(x)\psi(x)$  and  $\frac{d^n}{dx^n}\psi(x) = \psi_n(x)$  in terms of polygamma functions  $\psi_m(x)$  and “knows” how to evaluate polygamma functions at integer arguments, e.g.  $\psi(1) = -\gamma$  and  $\psi_n(1) = (-)^{n+1}n!\zeta(n+1)$ .

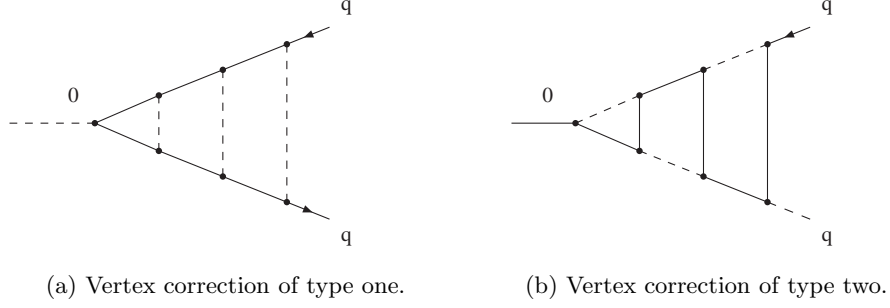


Figure 2: The two types of vertex corrections.

The functions  $\Gamma^1$  and  $\Gamma^2$  represent the two types of vertex corrections shown in figure 2.

The indices  $i$  and  $j$  give the number of subdivergences at different lines:

- $\Sigma_{i,j}$ :  $i$  = number of subdivergences at the fermion line,  
 $j$  = number of subdivergences at the boson line.
- $\Pi_{i,j}$ :  $i$  = number of subdivergences at the lower fermion line,  
 $j$  = number of subdivergences at the upper fermion line.
- $\Gamma_{i,j}^1$ :  $i$  = number of fermion self-energies and vertex corrections  
plugged into the zmt vertex and the internal edges connected to it,  
 $j$  = number of subdivergences at the boson line not connected to this vertex.
- $\Gamma_{i,j}^2$ :  $i$  = number of fermion or boson self-energies and vertex corrections  
plugged into the zmt vertex and the internal edges connected to it,  
 $j$  = number of fermion self-energies at the fermion line not connected to  
the vertex of zmt.

To denote complete graphs, we introduce additional functions  $\Sigma_{[i,j]}$ ,  $\Pi_{[i,j]}$  and  $\Gamma_{[i,j,k]}$  which notate the different kinds of subdivergences (cf.  $\Sigma_{[0,0]}$  in (4)). The indices count for  $\Sigma_{[i,j]}$  and  $\Pi_{[i,j]}$  as the indices in their corresponding characterizing functions given above. For vertex corrections of type one and two, the notation  $\Gamma_{[i,j,k]}$  denotes the three types of insertions in the following way:  $i$  insertions of self-energies at the edges connected to the zero momentum vertex,  $j$  insertions of self-energies at the edge not connected to that vertex, and  $k$  insertions of vertex corrections at the zmt vertex. Table 1 gives examples.

## 2.2 QED

The main difference stem from the presence of a gauge parameter  $\xi$  in the photon propagator and from the  $-ie\gamma_\mu$  vertex which make the calculations more difficult. In fact, as we will see, we will have to deal with matrices for the vertex corrections [10]. Nevertheless, the structure for the translation of a graph to an analytical result will be similar to what we had in Yukawa theory. Hence we will mainly give the results and just list the relevant changes.

### 2.2.1 Vacuum polarization

We will only consider one-loop photon self-energies, vacuum polarizations, as in our restricted class of Feynman graphs we can not construct a gauge invariant set of vacuum polarizations at higher loop orders.

---

	$\Sigma_{[0,0]}(q^2) = (-ig)^2 \Sigma_{0,0}[q^2]^{-\varepsilon} \not{q}$
	$\Sigma_{[1,0]}(q^2) = (-ig)^4 \Sigma_{1,0} \Sigma_{0,0}[q^2]^{-2\varepsilon} \not{q}$
	$\Sigma_{[2,1]}(q^2) = (-ig)^8 \Sigma_{2,1} \Pi_{0,0}(\Sigma_{0,0})^2[q^2]^{-4\varepsilon} \not{q}$
	$\Pi_{[0,0]}(q^2) = (-ig)^2 \Pi_{0,0}[q^2]^{-\varepsilon} q^2$
	$\Pi_{[2,1]}(q^2) = (-ig)^8 \Pi_{2,1} \Sigma_{1,0}(\Sigma_{0,0})^2[q^2]^{-4\varepsilon} q^2$
	$\Gamma_{[0,0,0]}^1(q^2) = (-ig)^3 \Gamma_{0,0}^1[q^2]^{-\varepsilon}$
	$\Gamma_{[0,0,2]}^1(q^2) = (-ig)^7 \Gamma_{2,0}^1 \Gamma_{1,0}^1 \Gamma_{0,0}^1[q^2]^{-3\varepsilon}$
	$\Gamma_{[2,0,0]}^1(q^2) = (-ig)^7 \Gamma_{2,0}^1 \Sigma_{1,0} \Sigma_{0,0}[q^2]^{-3\varepsilon}$
	$\Gamma_{[0,1,0]}^1(q^2) = (-ig)^5 \Gamma_{0,1}^1 \Pi_{0,0}[q^2]^{-2\varepsilon}$
	$\Gamma_{[0,0,0]}^2(q^2) = (-ig)^3 \Gamma_{0,0}^2[q^2]^{-\varepsilon}$
	$\Gamma_{[0,0,2]}^2(q^2) = (-ig)^7 \Gamma_{2,0}^2 \Gamma_{1,0}^2 \Gamma_{0,0}^2[q^2]^{-3\varepsilon}$
	$\Gamma_{[1,1,1]}^2(q^2) = (-ig)^9 \Gamma_{3,0}^2 \Gamma_{1,1}^2(\Sigma_{0,0})^2[q^2]^{-4\varepsilon}$

---

Table 1: Some examples how self-energy and vacuum polarization graphs are built up in Yukawa theory.

### 2.2.2 Fermion self-energy

The fermionic propagator in QED with insertions at the fermionic and photonic lines demands  $\tilde{\Sigma}$ :

$$\begin{aligned}
\tilde{\Sigma}_{i,j} = & \frac{1}{2} [(2-D) F_{j\varepsilon,1+i\varepsilon} - (3-D) F_{1+j\varepsilon,i\varepsilon} - (3-D) F_{1+j\varepsilon,1+i\varepsilon} \\
& + F_{2+j\varepsilon,-1+i\varepsilon} - 2 F_{2+j\varepsilon,i\varepsilon} + F_{2+j\varepsilon,1+i\varepsilon}] (1 - \delta_{0,j}) \\
& + [(2-D) \Sigma_{i,0} + \xi \Sigma'_{i,0}] \delta_{0,j},
\end{aligned} \tag{9}$$

with

$$\Sigma_{i,0} = \frac{1}{2} [F_{1+i\varepsilon,1} + F_{i\varepsilon,1}] \tag{10}$$

$$\Sigma'_{i,0} = \frac{1}{2} [F_{-1+i\varepsilon,2} - 2F_{i\varepsilon,2} - F_{i\varepsilon,1} + F_{1+i\varepsilon,2} - F_{1+i\varepsilon,1}]. \tag{11}$$

The appearance of the Kronecker  $\delta_{0,j}$  is obvious from the fact that the presence of one-loop vacuum polarizations in the internal photon line forces transversality of that propagation.

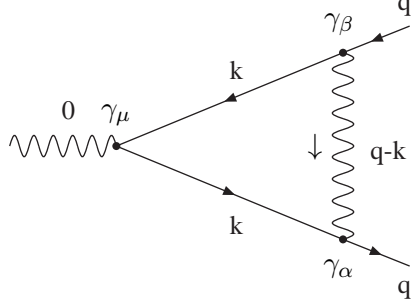


Figure 3: One-loop contribution to the vertex correction.

### 2.2.3 Vertex corrections

The most important difference to the Yukawa theory occurs in this part of the calculation. Consider the one-loop vertex correction in QED for vertex graphs as shown in Fig. 3.

The external structure of the vertex consists of two form factors: One for  $\gamma_\mu$  and one for  $\frac{q_\mu \not{q}}{q^2}$ , as  $\Gamma_\mu(0, q, q) = F_1(q^2)\gamma_\mu + F_2(q^2)\frac{q_\mu \not{q}}{q^2}$ . In the previous calculations, every subdivergence just caused an change in the exponent of various momenta in denominators of the integrals, resulting in non-integral exponents in equation (1). Now the result has two form factors  $F_1, F_2$  that emerge through the evaluation of a subgraph in a “bigger” graph. We will administer the two form factors in a matrix notation in accordance with [10]. We will need two-by-two matrices. The four entries determine four functions  $\Delta_{a,b}^{(i,j)}$ . Here,  $a, b \in \{1, 2\}$  and  $(i, j)$  count the number of internal insertions as before. The case  $b = 1$  corresponds to an internal vertex  $\gamma_\mu$ , the case  $b = 2$  corresponds to an internal vertex  $q_\mu \not{q}/q^2$  (where  $q$ , say, is the momentum flowing through this zero-momentum transfer vertex), while the index  $a$  enumerates the two possible form factors in the result. The result for the one-loop graph of Fig.3 is then

$$\left[ \Delta_{1,1}^{(0,0)} \gamma_\mu + \Delta_{2,1}^{(0,0)} \frac{q_\mu \not{q}}{q^2} \right] [q^2]^{-\varepsilon}.$$

For the two-loop graph shown in figure 4 we find

$$\Gamma_{[0,0,1]} = \left[ \left( \Delta_{11}^{(0,0)} \Delta_{11}^{(1,0)} + \Delta_{21}^{(0,0)} \Delta_{12}^{(1,0)} \right) \gamma_\mu + \left( \Delta_{11}^{(0,0)} \Delta_{21}^{(1,0)} + \Delta_{21}^{(0,0)} \Delta_{22}^{(1,0)} \right) \frac{q_\mu \not{q}}{q^2} \right] [q^2]^{-2\varepsilon}. \quad (12)$$

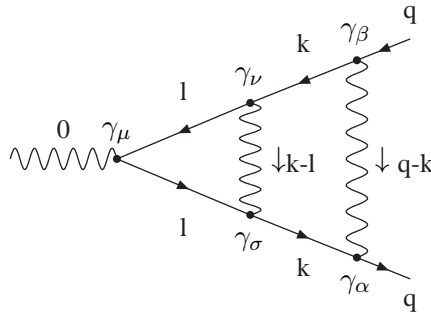


Figure 4: Two-loop contribution to the vertex correction.

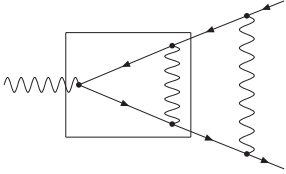


The multiplication of the  $\Delta_{kl}^{(i,j)}$  can be reformulated as a matrix multiplication. We define the general matrix (the upper index refers to the two cases of vertex corrections which we consider, we omit that index for simplicity in the matrix entries):

$$M_{i,j}^1 := \begin{pmatrix} \Delta_{11}^{(i,j)} & \Delta_{12}^{(i,j)} \\ \Delta_{21}^{(i,j)} & \Delta_{22}^{(i,j)} \end{pmatrix}$$

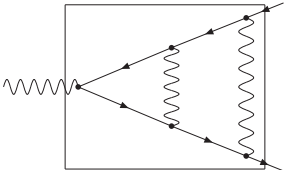
To each part of a graph which has the form of a vertex correction we assign a matrix. In this case of vertex corrections of type one, as in 2.a, the index  $i$  is the total number of subdivergences at the fermionic line (with no difference if it is of the form  $\Sigma$  or  $\Gamma$ ) and  $j$  the number of subdivergences at the photon line, as in Yukawa theory. One multiplies the matrices for the different divergent parts of a graph, starting from the innermost vertex correction which contains the vertex of  $\text{zmt}$ , and the corresponding matrix has zero entries in the second column obviously.

Let us make this clear with the help of our example of the two-loop vertex correction again. For the graph of figure 4 this means that we begin with the inner vertex correction marked with a box:



$$\equiv M_{0,0}^1 = \begin{pmatrix} \Delta_{11}^{(0,0)} & 0 \\ \Delta_{21}^{(0,0)} & 0 \end{pmatrix}$$

and then multiply this with the matrix for the outer vertex correction, which has one vertex correction as a subdivergence:



$$\equiv M_{1,0}^1 = \begin{pmatrix} \Delta_{11}^{(1,0)} & \Delta_{12}^{(1,0)} \\ \Delta_{21}^{(1,0)} & \Delta_{22}^{(1,0)} \end{pmatrix}$$

$$\Rightarrow \begin{pmatrix} \Delta_{11}^{(1,0)} & \Delta_{12}^{(1,0)} \\ \Delta_{21}^{(1,0)} & \Delta_{22}^{(1,0)} \end{pmatrix} \begin{pmatrix} \Delta_{11}^{(0,0)} & 0 \\ \Delta_{21}^{(0,0)} & 0 \end{pmatrix} = \begin{pmatrix} \Delta_{11}^{(1,0)}\Delta_{11}^{(0,0)} + \Delta_{12}^{(1,0)}\Delta_{21}^{(0,0)} & 0 \\ \Delta_{21}^{(1,0)}\Delta_{11}^{(0,0)} + \Delta_{22}^{(1,0)}\Delta_{21}^{(0,0)} & 0 \end{pmatrix}. \quad (13)$$

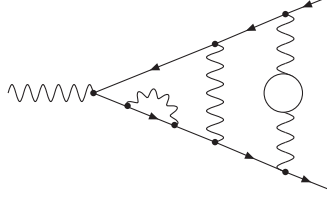
Multiplying (13) with  $(1,0)^T [q^2]^{-2\varepsilon}$ , we get the result as the column vector

$$\begin{pmatrix} (\Delta_{11}^{(1,0)}\Delta_{11}^{(0,0)} + \Delta_{12}^{(1,0)}\Delta_{21}^{(0,0)})[q^2]^{-2\varepsilon} \\ (\Delta_{21}^{(1,0)}\Delta_{11}^{(0,0)} + \Delta_{22}^{(1,0)}\Delta_{21}^{(0,0)})[q^2]^{-2\varepsilon} \end{pmatrix},$$

where in general the “upper” entry of this vector is the form factor  $F_1(q^2)$  belonging to  $\gamma_\mu$  and the “lower” one the form factor  $F_2(q^2)$  belonging to  $\frac{q^\mu \not{q}}{q^2}$ .

Subdivergences that are *not* vertex corrections given by  $\Sigma_{i,j}$  and  $\Pi_{i,j}$  are multiplied with a unit matrix and inserted in the string of matrices in front of the matrix of the vertex correction which they are part of. They increase subscripts  $i, j$  accordingly in that matrix.

As an example we get for the following graph:



$$\begin{aligned}
&\equiv \begin{pmatrix} \Delta_{11}^{(2,1)} & \Delta_{12}^{(2,1)} \\ \Delta_{21}^{(2,1)} & \Delta_{22}^{(2,1)} \end{pmatrix} \begin{pmatrix} \Pi_{0,0} & 0 \\ 0 & \Pi_{0,0} \end{pmatrix} \begin{pmatrix} \Delta_{11}^{(1,0)} & \Delta_{12}^{(1,0)} \\ \Delta_{21}^{(1,0)} & \Delta_{22}^{(1,0)} \end{pmatrix} \begin{pmatrix} \tilde{\Sigma}_{0,0} & 0 \\ 0 & \tilde{\Sigma}_{0,0} \end{pmatrix} \\
&\equiv M_{2,1}^1 \Pi_{0,0} M_{1,0}^1 \tilde{\Sigma}_{0,0}.
\end{aligned}$$

As already mentioned, the indices  $i$  and  $j$  count for QED vertex corrections of type one,  $\Gamma_{[i,j,k]}^1$ , similar to the ones defined for Yukawa vertex corrections of this type. Similarly, the indices for the type two vertex corrections  $\Gamma_{[i,j,k]}^2$  in QED count as in Yukawa type two. And the matrix multiplication described above stays the same apart from different entries for the matrices, which can be readily calculated in terms of functions  $F_{a,b}$ . We do not list the two sets of four functions  $\Delta_{a,b}^{(i,j)}$  in terms of  $F_{c,d}$  functions explicitly, but the interested reader can find them from our publicly available programs [12]. Table 2 shows some examples how graphs are built in QED.

### 3 Renormalization

Renormalization employs a simple principle of multiplicative subtraction, making use of the underlying Hopf algebra structure of Feynman graphs [14, 4]: the coproduct

$$\Delta(\Gamma) = \Gamma \otimes 1 + 1 \otimes \Gamma + \sum_{\gamma \subset \Gamma} \gamma \otimes \Gamma/\gamma$$

and antipode

$$S(\Gamma) = -\Gamma - \sum_{\gamma \subset \Gamma} \gamma \Gamma/\gamma$$



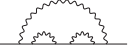


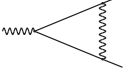
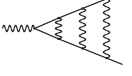
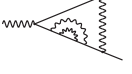
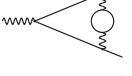



are the structure maps which allow the construction of counterterms and renormalized quantities. One employs Feynman rules  $\phi : H \rightarrow V$  as an element in the group of characters of the Hopf algebra  $H$ , with target space  $V$  (a suitable ring or algebra) and makes the target space into a Baxter algebra  $(V, R)$  by choosing a renormalization map  $R$  such that  $R(ab) + R(a)R(b) = R(aR(b)) + R(R(a)b)$ . One then has the counterterm

$$S_R^\phi(\Gamma) = -R[\phi(\Gamma) + \sum_{\gamma \subset \Gamma} S_R^\phi(\gamma)\phi(\Gamma/\gamma)]$$

and a further recursion delivers the renormalized result

$$S_R^\phi \star \phi(\Gamma) = S_R^\phi(\Gamma) + \phi(\Gamma) + \sum_{\gamma \subset \Gamma} S_R^\phi(\gamma)\phi(\Gamma/\gamma).$$

---

	$\tilde{\Sigma}_{[0,0]}(q^2) = (-ie)^2 \tilde{\Sigma}_{0,0}[q^2]^{-\varepsilon} \not{q}$
	$\tilde{\Sigma}_{[1,0]}(q^2) = (-ie)^4 \tilde{\Sigma}_{1,0} \tilde{\Sigma}_{0,0}[q^2]^{-2\varepsilon} \not{q}$
	$\tilde{\Sigma}_{[2,0]}(q^2) = (-ie)^6 \tilde{\Sigma}_{2,0} \tilde{\Sigma}_{0,0} \tilde{\Sigma}_{0,0}[q^2]^{-3\varepsilon} \not{q}$
	$\tilde{\Sigma}_{[2,1]}(q^2) = (-ie)^8 \tilde{\Sigma}_{2,1} \Pi_{0,0} (\tilde{\Sigma}_{0,0})^2 [q^2]^{-4\varepsilon} \not{q}$
	$\Pi_{[0,0]}(q^2) = (-ie)^2 [q^2]^{-\varepsilon} \Pi_{0,0} \left[ g^{\mu\nu} - \frac{q^\mu q^\nu}{q^2} \right] q^2$
	$\Gamma_{[0,0,0]}^1(q^2) = (-ie)^3 M_{0,0}^1 [q^2]^{-\varepsilon}$
	$\Gamma_{[0,0,2]}^1(q^2) = (-ie)^7 M_{2,0}^1 M_{1,0}^1 M_{0,0}^1 [q^2]^{-3\varepsilon}$
	$\Gamma_{[2,0,0]}^1(q^2) = (-ie)^7 M_{2,0}^1 \tilde{\Sigma}_{1,0} \tilde{\Sigma}_{0,0} [q^2]^{-3\varepsilon}$
	$\Gamma_{[0,1,0]}^1(q^2) = (-ie)^5 M_{0,1}^1 \Pi_{0,0} [q^2]^{-2\varepsilon}$
	$\Gamma_{[0,0,0]}^2(q^2) = (-ig)^3 M_{0,0}^2 [q^2]^{-\varepsilon}$
	$\Gamma_{[0,0,2]}^2(q^2) = (-ig)^7 M_{2,0}^2 M_{1,0}^2 M_{0,0}^2 [q^2]^{-3\varepsilon}$
	$\Gamma_{[1,1,1]}^2(q^2) = (-ie)^9 M_{3,0}^2 M_{1,1}^2 (\tilde{\Sigma}_{0,0})^2 [q^2]^{-4\varepsilon}$

---

Table 2: Some examples how self-energy and vacuum polarization graphs are built up in QED.

The counterterm  $S_R^\phi$  is in the image of  $R$ , while  $\phi(\Gamma) + \sum_{\gamma \subset \Gamma} S_R^\phi(\gamma) \phi(\Gamma/\gamma)$  is the result of Bogoliubov's famous  $\overline{R}(\Gamma)$  operation on  $\Gamma$  which eliminates subdivergences in  $\Gamma$  [13].

Under suitable conditions on the behavior of  $R$ , in this ratio of characters short distance singularities drop out [14, 15].

Before we comment on the renormalization scheme chosen for our calculations, let us introduce the bidegree of a Feynman graph. This standard notion can be introduced for any Hopf algebra which is reduced to scalars [7, 4] by the counit  $\bar{e}$  with

$$\bar{e}(q1) = q, \bar{e}(X) = 0, \text{ else.}$$

If we decompose  $H = H_0 \oplus H_{\text{aug}}$ , with  $H_{\text{aug}}$  being the augmentation ideal as the kernel of  $\bar{e}$  we can investigate, for any positive integer  $k$  and Hopf algebra element  $X$ ,

$$X_k := \Delta^{k-1}(X) \cap H_{\text{aug}}^{\otimes k}.$$

For sufficiently large  $k$  this will necessarily vanish. We define the bidegree  $\text{bid}(X)$  as the largest  $k$  such that  $X_k \neq 0$ . Elements in  $H_0$  have bidegree zero. Note that Hopf algebra elements of unit bidegree are precisely the primitive elements  $X \in H_{\text{aug}}$  in the Hopf algebra, with

$$\Delta(X) = X \otimes 1 + 1 \otimes X \notin H_{\text{aug}} \otimes H_{\text{aug}}.$$

Having introduced this standard notion we introduce the renormalization scheme for which we choose minimal subtraction (MS). Each application of the scheme is given by a projection onto the pole-part of the considered Laurent series and is symbolized with brackets “ $\langle \rangle$ ”:

$$\langle \sum_{j=-r}^{+\infty} c_j \varepsilon^j \rangle = \sum_{j=-r}^{-1} c_j \varepsilon^j.$$

The reader should convince himself that this map makes the ring of Laurent series with poles of finite order into a Baxter algebra,

$$\langle ab \rangle + \langle a \rangle \langle b \rangle = \langle a \langle b \rangle \rangle + \langle \langle a \rangle b \rangle.$$

Note that the degree  $r$  of the pole terms in a Laurent series assigned to a graph by the Feynman rules in dimensional regularization is in general majorized by the bidegree  $r \leq \text{bid}(\Gamma)$  and equals the bidegree in our simple applications.

We expect to encounter  $\zeta(n)$  inside the coefficients of the Laurent series in the regularization parameter  $\varepsilon$  emerging from a series expansion of the functions  $F_{a,b}$ .

In QED we have to take our matrix-calculus into account. The renormalization of such matrix expressions is now given by inserting a diagonal matrix  $R$ , which consists of the renormalization map as entries:

$$R := \begin{pmatrix} R_{MS} & 0 \\ 0 & R_{MS} \end{pmatrix}$$

Inside a string of matrices, this matrix has to be inserted wherever the renormalization map is applied. It acts on expressions on the right.

## 4 Rooted Trees

Before we build up graphs and calculate their counterterms, ie. their antipodes, let us first mention that in our simplified context, the Hopf algebra of Feynman graphs is isomorphic to a Hopf algebra of rooted trees with a very small set of decorations given by our one-loop graphs.

In the class of graphs to which we have restricted ourselves one-particle irreducible subgraphs are either nested in each other, or disjoint. They hence form tree-like hierarchies, and one easily translates graphs in rooted trees [15], with a one-to-one correspondence between one-particle irreducible subgraphs and vertices in the rooted tree (the map from graphs to rooted trees is one-to-many for overlapping divergent graphs, and can be systematically constructed [16]):

The translation from a Feynman diagram to a rooted tree has to be done in the following way: *Set a box around the subdivergences of a Feynman graph  $\Gamma$  and mark the upper horizontal line with a dot ( $\simeq$  vertex). Dots of nested boxes, that is boxes where one of them is contained inside the other, are connected with a line ( $\simeq$  edge) (see fig. 5).*

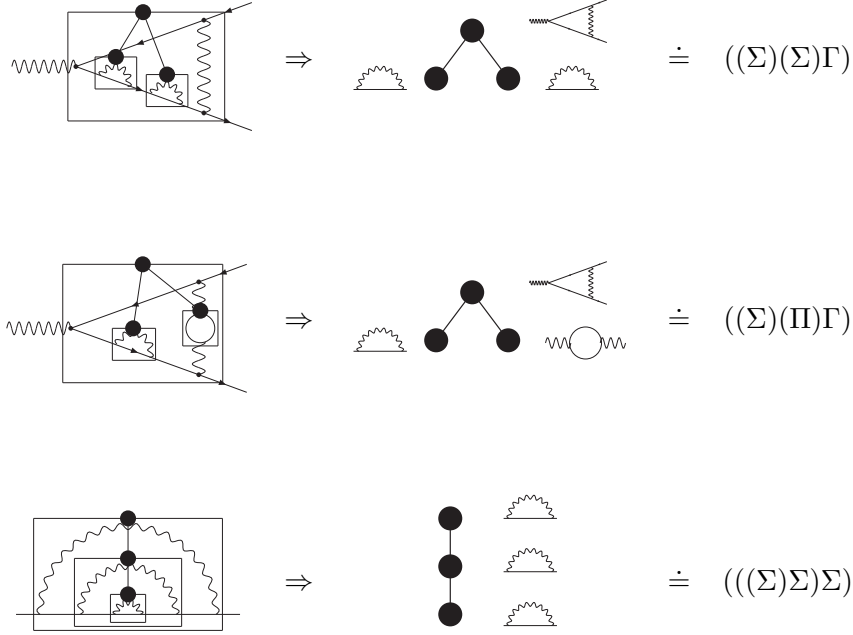


Figure 5: Translation of Feynman diagrams into rooted trees. Here we are dealing with decorated rooted trees, where the subdivergences are written next to the vertex to which they belong. In the last column one can see another way to encode the structure of the trees in the form of nested lists [14]: The entries are again the divergent parts of a Feynman diagram and the formation of the parentheses gives the structure of the tree, beginning with the vertices “at the end” of a tree up to the root.

Each vertex of such a tree represents a divergent subgraph of the diagram. The antipode of such a tree is a sum over all *full cuts* or, recursively, iterates over admissible cuts using the coproduct. This easy-to-implement [2] coproduct

$$\Delta(T) = T \otimes 1 + 1 \otimes T + \sum_{\text{admissible cuts } c} P^c(T) \otimes R^c(T)$$

is by now a standard combinatorial tool (see, for example [15]). Using it, the counterterm is a recursive construct

$$S_{MS}(T) = -\langle T(\Gamma) + \sum_{\text{admissible cuts } c} S_{MS}(P^c(T))R^c(T) \rangle,$$

where an evaluation of the graph corresponding to the tree using the Feynman rules is understood before applying the projection  $\langle \rangle$  for minimal subtraction (MS), in accordance with the general formula given for graphs.

## 5 Implementation

We shortly describe an implementation of our scheme in a computer program. This implementation is not entirely self-contained in the sense that given a Feynman diagram, it would compute the antipode. Instead, its input is a decorated rooted tree in list notation such as

$(\Gamma(\Pi)(\Sigma))$ . The actual construction of that rooted tree from the diagram, as described in section 4 is left to the user (see also fig. 5).

Our implementation uses the GiNaC system for symbolic computation in the C++ programming language [1]. GiNaC provides efficient implementations for handling Laurent series as needed in dimensional regularization. From C++, all the linguistic instruments for object-oriented programming are borrowed and available to us. We follow a traditional approach for representation of our rooted trees where there exists a container class called `node` that may or may not have several children of the same class. In addition, each vertex in an object of class `node` contains an object of the abstract and polymorphic class `decoration`. From the abstract `decoration` class a number of concrete classes like `Sigma`, `Gamma` and `Vacuum` are derived, corresponding to primitive Feynman diagrams  $\Sigma$ ,  $\Gamma$  and  $\Pi$ , as well as some additional classes that allow us to distinguish between the position of a subgraph inside its supergraph.

The trees under consideration are not ordered with respect to their children, i.e. the trees  $(\Gamma(\Sigma)(\Pi))$  and  $(\Gamma(\Pi)(\Sigma))$  are equivalent. Therefore the children form a multiset where only the multiplicity of occurrences is relevant.

A template class `multiset` is part of the C++ Standard Template Library (STL). It has the additional advantage that the elements are always automatically sorted with respect to some specified ordering. This turns out to be useful for convenient identification of equivalent nodes and also to establish an order relation on them. The state of the edges leading to the children of a node (either “cut” or “uncut”) needs to be taken into account as well, so the multiset is really one of pairs of nodes and boolean variables. We chose to delegate methods from class `node` to the corresponding class derived from `decoration` using dynamic type-dispatch. Hence, the decoration must be stored as a pointer, calling for some hand-made memory management in class `node`. A completely realistic layout of our class `node` is then:

```

1  class node {
2  public:
3      // constructors, destructors, delegators,
4      // etc ...
5  private:
6      decoration *deco;
7      multiset< pair< node, bool > > children;
8  };

```

Note that a `node` can be either the entire tree, or a subtree or a single (atomic) leaf. The layout of class `decoration` holds a pair of indices and in the case of QED a GiNaC expression (class `ex`) for the gauge. An object of class `ex` is entirely sufficient, since it may contain either a numerical value (integer or fractional) or a symbol (like  $\xi$ ) (or even more complex expressions, if need should arise).

The knowledge how to manipulate the indices  $i$  and  $j$ , depending on the type of decoration and on the state of the edges is built into the classes of type `decoration`. They are automatically adjusted when the tree is constructed. Furthermore, the state of the edges is also irrelevant for the user of the program since we need all possible combinations of cuts. If there are  $n$  vertices inside a tree, then there are  $n - 1$  edges and we have to construct all possible  $2^{n-1}$  combinations.

Once all the trees have been created we call a method called `evaluate` in each of them that traverses the tree in a top-down fashion: In each node, the expression in terms of  $F_{a+i\varepsilon, b+j\varepsilon}$  is dispatched and expanded as a series in the regularization parameter  $\varepsilon$  before `evaluate` is called on the multiset of children. The resulting  $2^{n-1}$  Laurent series are then added together and the coefficients are expanded. This procedure yields the antipode.

Here is an example how the programs are used in practice:

```

1 $ ./qed1 "(((Sigma[0])(Sigma[xi])Gamma[-1])Gamma[xi])"
2 After decoration the tree has these indices:
3 (Gamma[3,0][xi](Gamma[2,0][-1](Sigma[0,0][0])(Sigma[0,0][xi])))
4 ----+----#----+----#----+----#----+----#----+----#----+----#
5 The antipode of this tree is:
6
7 (-1/4-1/4*xi^2-1/2*xi)*x^(-3)
8 +(7/24+1/24*xi^2+1/3*xi)*x^(-2)
9 +(-5/16-13/48*xi^2-7/12*xi)*x^(-1)

```

The graph to be computed is passed in tree form as a string on the command line, together with the gauge parameter. Note how the indices  $i$  and  $j$  are then set up automatically in line 3. The next line is a simple progress bar, useful when computations become longer. The result is then printed as a power series in the regularization parameter, called  $x$  instead of  $\varepsilon$  in order to please the computer.

Computationally, the results are always quite small (c.f. section 6) but there is a huge swell of intermediate expressions. After all, the Laurent series arise from expanding products and sums of lots of  $\Gamma$ -functions and so inevitably carry Euler-Mascheroni constants. But these have to vanish by cancellations, a fact that is conveniently used as a consistency check for the result. In practice, antipodes of nine-loop graphs in massless QED are still computationally feasible but may require several hours and hundreds of megabytes memory. This emphasizes the drastic loss of efficiency in comparison with [2, 3], which is compensated by a gain in flexibility to handle different decorations at any step in the recursion.

The programs developed herein are written in plain ISO C++ [17] and will run on any system where the GiNaC library has been ported to. Note that porting to a new platform will require porting CLN [18] to that platform first, since GiNaC depends on CLN for its arbitrary precision arithmetic.

## 6 Computational Results

In a first step, to examine the appearance of  $\zeta$ -functions, we will now calculate the antipode of different graphs given in figure 6 and figure 7 that represent the two topologies of figure 1. In Yukawa theory the graphs  $\Gamma_{[1,1,1]}^1$  and  $\Gamma_{[1,1,1]}^2$  of figure 6 are representations of the ladder topology 1.b, the graphs  $\Gamma_{[2,0,1]}^1$  and  $\Gamma_{[2,0,1]}^2$  of the swiss cheese topology 1.a. The same holds for QED with  $[1, 1, 1]$  replaced by  $[1, 1, 2]$  and  $[2, 0, 1]$  by  $[2, 0, 2]$ .

The graphs for the Yukawa theory, together with their expressions in characterizing functions are given in figure 6. The figure also contains the decorated rooted trees we get from them to calculate the antipode. One can see that except from the decorations they all belong to the same rooted tree, and hence have the same structure as far as their short distance singularities go, as advertised in the introduction.

In QED, the considered graphs in figure 7 possess one more vertex correction compared to the graphs in yukawa theory. This additional photon line is necessary because the short distance singularity structure is actually determined by the bidegree, ie. the number of subdivergent graphs. It so happens in QED that the one-loop fermion self-energy and one-loop vertex corrections (with divergent subgraphs) are overall finite if the internal photon is transversal. In our case, we thus find that the insertion of a one-loop vacuum polarization into the internal photon line in a vertex results in a convergent vertex correction. We have to plug the whole

$\Gamma_{[1,1,1]}^1 \equiv$		$\equiv (-ig)^9 \Gamma_{3,0}^1 \Gamma_{1,1}^1 \Sigma_{0,0} \Pi_{0,0} [q^2]^{-4\epsilon}$
$\Gamma_{[1,1,1]}^2 \equiv$		$\equiv (-ig)^9 \Gamma_{3,0}^2 \Gamma_{1,1}^2 \Sigma_{0,0} \Sigma_{0,0} [q^2]^{-4\epsilon}$
$\Gamma_{[2,0,1]}^1 \equiv$		$\equiv (-ig)^9 \Gamma_{3,0}^1 \Gamma_{2,0}^1 \Sigma_{0,0} \Sigma_{0,0} [q^2]^{-4\epsilon}$
$\Gamma_{[2,0,1]}^2 \equiv$		$\equiv (-ig)^9 \Gamma_{3,0}^2 \Gamma_{2,0}^2 \Sigma_{0,0} \Sigma_{0,0} [q^2]^{-4\epsilon}$

--	--

Figure 6: Graphs in Yukawa theory and their decorated rooted trees.

function into one more vertex correction to get to the next level in the bidegree. And indeed, we need an additional vertex correction, compared to Yukawa theory, to obtain the  $\zeta(3)$  in the pole-terms: gauge symmetry delays the appearance of transcendentals [19]. Also let us mention that we can easily compare graphs which have an internal vacuum polarization with graphs which have an internal fermion self-energy by using the before-mentioned elimination of the trace in the vacuum polarization, using

$$\Pi_{0,0} = \text{tr}(\mathbf{1}) \frac{1}{2} F_{1,1} = \text{tr}(\mathbf{1}) \Sigma_{0,0}.$$

Furthermore,  $\Gamma_{[1,1,2]}^2$  and  $\Gamma_{[2,0,2]}^2$  in QED do not have this extra shift between loop number and bidegree by themselves, as there the desire to maintain the same topology never forces us to use a vacuum polarization as a subgraph: all one-loop subdivergences are fermion self-energies and vertex corrections. However, we use the same gauges in these graphs as in the graphs



$\Gamma_{[1,1,2]}^1 \equiv$		$\equiv (-ie)^{11} M_{4,0}^1 M_{3,0}^1 M_{1,1}^1 \tilde{\Sigma}_{0,0} \Pi_{0,0} [q^2]^{-5\epsilon}$
$\Gamma_{[1,1,2]}^2 \equiv$		$\equiv (-ie)^{11} M_{4,0}^2 M_{3,0}^2 M_{1,1}^2 \tilde{\Sigma}_{0,0} \tilde{\Sigma}_{0,0} [q^2]^{-5\epsilon}$
$\Gamma_{[2,0,2]}^1 \equiv$		$\equiv (-ie)^{11} M_{4,0}^1 M_{3,0}^1 M_{2,0}^1 \tilde{\Sigma}_{0,0} \tilde{\Sigma}_{0,0} [q^2]^{-5\epsilon}$
$\Gamma_{[2,0,2]}^2 \equiv$		$\equiv (-ie)^{11} M_{4,0}^2 M_{3,0}^2 M_{2,0}^2 \tilde{\Sigma}_{0,0} \tilde{\Sigma}_{0,0} [q^2]^{-5\epsilon}$

Figure 7: Graphs in QED and their decorated rooted trees.

$\Gamma_{[1,1,2]}^1$  and  $\Gamma_{[2,0,2]}^1$  to compare the results directly (see below), and therefore obtain the same difference between loop-number and bidegree.

Finally, in our results, we are only interested in residues of counterterms, poles of first order. All interesting relations between transcendental degree and topology will appear there. The scattering type formula [4] will make sure that parts of these relations will then resurface in the poles of higher order in the counterterm, but they contain no new information. So in the following we solely exhibit the residues of the counterterms for our selected class of graphs. We denote by  $\text{res}(\Gamma)$  this coefficient of the pole of first order in the MS counterterm in dimensional regularization of a graph  $\Gamma$ . Assorted results for these residues are:

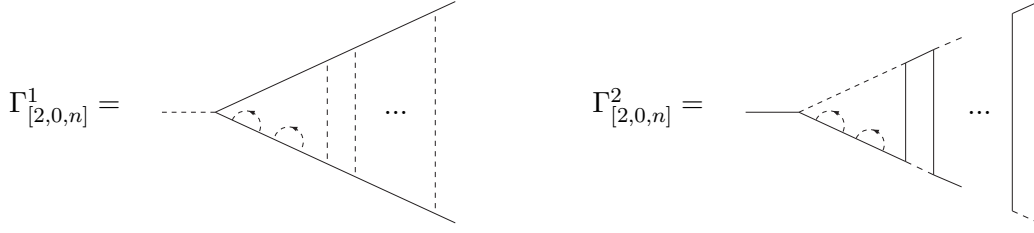


Figure 8: Iterated vertex corrections.

Yukawa theory:

$$\begin{aligned}
\text{res}(\Gamma_{[1,1,1]}^1) &= \frac{5}{48} \\
\text{res}(\Gamma_{[1,1,1]}^2) &= \frac{1}{24} \\
\text{res}(\Gamma_{[2,0,1]}^1) &= \left( \frac{5}{48} - \frac{1}{8}\zeta(3) \right) \\
\text{res}(\Gamma_{[2,0,1]}^2) &= \left( \frac{1}{12} - \frac{1}{8}\zeta(3) \right)
\end{aligned}$$

QED:

$$\begin{aligned}
\text{res}(\Gamma_{[1,1,2]}^1) &= - \left( \frac{1}{480}(301 + 143\xi - 170\xi^2) \right) \\
\text{res}(\Gamma_{[1,1,2]}^2) &= - \left( \frac{1}{960}(584 + 659\xi + 59\xi^2) \right) \\
\text{res}(\Gamma_{[2,0,2]}^1) &= - \left( \frac{1}{480}(521 + 309\xi - 236\xi^2) + \frac{3}{10}\zeta(3)(1 + \xi)^2 \right) \\
\text{res}(\Gamma_{[2,0,2]}^2) &= - \left( \frac{1}{960}(832 + 879\xi + 31\xi^2) + \frac{3}{10}\zeta(3)(1 + \xi)^2 \right)
\end{aligned}$$

We see, that in Yukawa theory the graphs  $\Gamma_{[2,0,1]}^1$  and  $\Gamma_{[2,0,1]}^2$  with the swiss cheese topology have a residue involving  $\zeta(3)$ , while  $\Gamma_{[1,1,1]}^1$  and  $\Gamma_{[1,1,1]}^2$  realizing the ladder topology just have a rational residue, as expected. A similar result holds in QED: the graphs  $\Gamma_{[2,0,2]}^1$  and  $\Gamma_{[2,0,2]}^2$  with the swiss cheese topology again have a residue involving  $\zeta(3)$ , while  $\Gamma_{[1,1,2]}^1$  and  $\Gamma_{[1,1,2]}^2$  realizing the ladder topology just have a rational residue. Those residues are in general a linear combination of terms of varying transcendental weight. This weight vanishes for a rational number, and in accordance with standard practice in the study of multiple zeta values the transcendental weight  $w$  of a monomial  $\prod_i \zeta(j_i)$  is

$$w\left(\prod_i \zeta(j_i)\right) = \sum_i j_i.$$

Then, the above results confirm that the coefficient of the highest weight transcendental in the transition from  $\text{res}(\Gamma_{[2,0,1]}^1)$  to  $\text{res}(\Gamma_{[2,0,1]}^2)$  ( $\text{res}(\Gamma_{[2,0,2]}^1)$  to  $\text{res}(\Gamma_{[2,0,2]}^2)$  for QED) is invariant. This is the partial symmetry announced in the introduction. It holds for any gauge in the

QED case and holds in general, if we increase the loop number as for example in figure (8).

In Yukawa theory we get:

$$\begin{aligned}
\text{res}(\Gamma_{[2,0,1]}^1) &= \left( \frac{5}{48} - \frac{1}{8}\zeta(3) \right) \\
\text{res}(\Gamma_{[2,0,1]}^2) &= \left( \frac{1}{12} - \frac{1}{8}\zeta(3) \right) \\
\text{res}(\Gamma_{[2,0,2]}^1) &= \left( \frac{1}{20} - \frac{9}{40}\zeta(3) - \frac{3}{80}\zeta(4) \right) \\
\text{res}(\Gamma_{[2,0,2]}^2) &= \left( \frac{1}{240} - \frac{1}{20}\zeta(3) - \frac{3}{80}\zeta(4) \right) \\
\text{res}(\Gamma_{[2,0,3]}^1) &= - \left( \frac{23}{90} + \frac{9}{20}\zeta(3) + \frac{7}{80}\zeta(4) + \frac{7}{240}\zeta(5) \right) \\
\text{res}(\Gamma_{[2,0,3]}^2) &= - \left( -\frac{1}{240} + \frac{1}{6}\zeta(3) + \frac{1}{80}\zeta(4) + \frac{7}{240}\zeta(5) \right) \\
\text{res}(\Gamma_{[2,0,4]}^1) &= - \left( \frac{919}{630} + \frac{71}{70}\zeta(3) + \frac{111}{560}\zeta(4) + \frac{1}{12}\zeta(5) + \frac{1}{560}\zeta(3)^2 + \frac{1}{112}\zeta(6) \right) \\
\text{res}(\Gamma_{[2,0,4]}^2) &= - \left( \frac{65}{224} + \frac{11}{140}\zeta(3) + \frac{1}{16}\zeta(4) + \frac{1}{120}\zeta(5) + \frac{1}{560}\zeta(3)^2 + \frac{1}{112}\zeta(6) \right) \\
\text{res}(\Gamma_{[2,0,5]}^1) &= - \left( \frac{6481}{1120} + \frac{33613}{13440}\zeta(3) + \frac{2133}{4480}\zeta(4) + \frac{101}{480}\zeta(5) + \frac{27}{4480}\zeta(3)^2 \right. \\
&\quad \left. + \frac{27}{896}\zeta(6) + \frac{3}{4480}\zeta(3)\zeta(4) + \frac{7}{1920}\zeta(7) \right) \\
\text{res}(\Gamma_{[2,0,5]}^2) &= - \left( \frac{863}{3360} + \frac{61}{160}\zeta(3) + \frac{27}{1120}\zeta(4) + \frac{7}{120}\zeta(5) + \frac{1}{2240}\zeta(3)^2 \right. \\
&\quad \left. + \frac{1}{448}\zeta(6) + \frac{3}{4480}\zeta(3)\zeta(4) + \frac{7}{1920}\zeta(7) \right)
\end{aligned}$$

Similarly, for QED we find:

$$\begin{aligned}
\text{res}(\Gamma_{[2,0,2]}^1) &= -\frac{1}{480}(521 + 309\xi - 236\xi^2) - \frac{3}{10}(1 + \xi)^2\zeta(3) \\
\text{res}(\Gamma_{[2,0,2]}^2) &= -\frac{1}{960}(832 + 879\xi + 31\xi^2) - \frac{3}{10}(1 + \xi)^2\zeta(3) \\
\text{res}(\Gamma_{[2,0,3]}^1) &= -\frac{1}{5760}(13377 + 16773\xi + 12091\xi^2 + 9463\xi^3) + \frac{1}{30}(1 + \xi)^2(-38 + 7\xi)\zeta(3) \\
&\quad - \frac{3}{40}(1 + \xi)^3\zeta(4) \\
\text{res}(\Gamma_{[2,0,3]}^2) &= -\frac{1}{5760}(13327 + 32578\xi + 26038\xi^2 + 6811\xi^3) - \frac{1}{60}(1 + \xi)^2(31 + 4\xi)\zeta(3) \\
&\quad - \frac{3}{40}(1 + \xi)^3\zeta(4)
\end{aligned}$$

$$\begin{aligned}
\text{res}(\Gamma_{[2,0,4]}^1) &= -\frac{1}{40320}(427681 + 1048812\xi + 889375\xi^2 + 130774\xi^3 - 145630\xi^4) \\
&\quad -\frac{1}{840}(1+\xi)^2(2551 + 425\xi + 736\xi^2)\zeta(3) + \frac{1}{280}(1+\xi)^3(-121 + 23\xi)\zeta(4) \\
&\quad -\frac{1}{20}(1+\xi)^4\zeta(5) \\
\text{res}(\Gamma_{[2,0,4]}^2) &= -\frac{1}{161280}(1357764 + 4016396\xi + 4028301\xi^2 + 1438370\xi^3 + 68749\xi^4) \\
&\quad -\frac{1}{1680}(1+\xi)^2(1448 + 2365\xi + 836\xi^2)\zeta(3) - \frac{1}{140}(1+\xi)^3(29 + 2\xi)\zeta(4) \\
&\quad -\frac{1}{20}(1+\xi)^4\zeta(5) \\
\text{res}(\Gamma_{[2,0,5]}^1) &= \frac{1}{430295040}(-19150607852 - 55087254529\xi - 55376777218\xi^2 - 24306202368\xi^3 \\
&\quad -10014576786\xi^4 - 5440770359\xi^5) \\
&\quad +\frac{1}{4480}(1+\xi)^2(-39057 - 40975\xi - 19389\xi^2 + 6061\xi^3)\zeta(3) \\
&\quad -\frac{3}{4480}(1+\xi)^3(2031 + 11\xi + 446\xi^2)\zeta(4) + \frac{1}{960}(1+\xi)^4(-347 + 67\xi)\zeta(5) \\
&\quad -\frac{3}{1120}(1+\xi)^5\zeta(3)^2 - \frac{3}{224}(1+\xi)^5\zeta(6) \\
\text{res}(\Gamma_{[2,0,5]}^2) &= -\frac{1}{1290240}(29658556 + 111493999\xi + 161539373\xi^2 + 112812993\xi^3 \\
&\quad +38688379\xi^4 + 5579364\xi^5) \\
&\quad -\frac{1}{26880}(1+\xi)^2(80770 + 155550\xi + 79521\xi^2 + 3472\xi^3)\zeta(3) \\
&\quad -\frac{1}{8960}(1+\xi)^3(3254 + 3919\xi + 1340\xi^2)\zeta(4) \\
&\quad -\frac{1}{960}(1+\xi)^4(179 + 8\xi)\zeta(5) \\
&\quad -\frac{3}{1120}(1+\xi)^5\zeta(3)^2 - \frac{3}{224}(1+\xi)^5\zeta(6)
\end{aligned}$$

The reader will note that in QED our residues are polynomials in the gauge parameter of a degree reduced by two steps from what one might expect, to enable comparison between configurations with insertions of self-energies into photon or fermion lines. The corresponding fermion self-energy was for that purpose evaluated in the Feynman gauge, and in the Landau gauge for the affected photon propagator. If one only compares cases with self-energy insertions at fermionic lines, one can abandon these restrictions and we did confirm that the reported invariance holds as expected with coefficients which are polynomials in the gauge parameter of degree equal to the number of photon lines.

## 7 Discussion and Proof

Actually, results of the form reported in the previous sections can be derived from the analytic structure of the functions  $F_{a,b}$  and some basic field theoretic arguments.

Let us reconsider the situation. The simplicity of Feynman graphs considered here manifests itself computationally by the fact that they factorize in a unique manner. Each divergent subgraph  $\gamma$  depends only on a single external momentum  $q$  say (that is the reason why we only consider vertex subgraphs at zmt), such that its evaluation in dimensional regularization gives a result of the form

$$\phi(\gamma)(\varepsilon) = [q^2]^{-n(\gamma)\varepsilon} \sum_i F_i(\varepsilon) c_i(q).$$

Here,  $n(\gamma)$  is the number of loops in  $\gamma$ , and  $F_i(\varepsilon)$  are  $q$ -independent form factors, and the dimensionless  $c_i(q)$  are

$c_1(q) = \gamma_\mu, c_2(q) = q_\mu \not{q}/q^2$  for the QED vertex (the only case here in which the sum has more than one term),

$c_1(q) = 1$  for the vertex correction in Yukawa theory,

$c_1(q) = \not{q}$  for any fermion self-energy,

$c_1(q) = g_{\mu\nu} - q_\mu q_\nu / q^2$  for the photon,

$c_1(q) = 1$  for the scalar boson.

Insertions of such graphs  $\gamma$  in another graph  $\Gamma$  only raises powers of the scalar part of some propagator of  $\Gamma$ :

$$\frac{1}{q^2} \rightarrow \frac{1}{[q^2]^{1+n(\gamma)\varepsilon}}.$$

We can keep track of this by notating these loop numbers  $n(\gamma)$  in the entries  $M(\Gamma)_{ij}$  for the corresponding propagator in the adjacency matrix  $M(\Gamma)$ .

Let us now assume that  $\Gamma$  is some primitive vertex correction, ie. free of divergent subgraphs, and let us write as before  $\Gamma^1$  and  $\Gamma^2$  for two distinct choices of zmt.

Consider a bunch of 1PI graphs  $X = \prod_{i=1}^k \gamma_i$  each dependent on a sole external momentum as described above. Let  $k = \text{bid}(X)$  be the bidegree of  $X$ , so that  $X$  has a highest pole in  $\varepsilon$  of degree  $k$  with coefficient  $c_k^X$ . Let now  $G_X$  be chosen gluing data such that  $\Gamma_X := \Gamma \star_{G_X} X$  is obtained from inserting  $X$  at specified vertices and propagators into  $\Gamma$ , with  $\text{bid}(\Gamma) = 1$  without loss of generality. (Any 1PI graph can be written in the form  $\Gamma \star_{G_X} X$  for appropriate such  $\Gamma, X$  [14, 16, 4], in generalization of the closed Hochschild one cocycle  $B_+$  of undecorated rooted trees). Further, each  $X$  allows for an expansion

$$\phi(X) = \frac{c_k^X}{\varepsilon^k} (1 + T(X)(\varepsilon))$$

and similarly, let  $\phi(\Gamma) = \frac{\text{res}(\Gamma)}{\varepsilon} (1 + T(\Gamma)(\varepsilon))$ . Now assume that the Taylor series  $[1 + T(X)(\varepsilon)][1 + T(\Gamma)(\varepsilon)] = 1 + \sum_{j=1}^{\infty} c_j \varepsilon^j$  is such that the transcendental weight  $w(c_j)$  of  $c_j$  increases with  $j$ :

$$w(c_j) < w(c_{j+1}),$$

$\forall j \geq k - 1$ . Here, we define the transcendental weight of an expression which is a sum of terms as the highest transcendental weight appearing in its terms.<sup>4</sup>

---

<sup>4</sup>The question as to how define the transcendental weight in a context which exceeds the Riemann  $\zeta$ -

**Proposition 1** *The counterterm is the same for  $\Gamma_X^1$  and  $\Gamma_X^2$ , and hence their residues are equal.*

Proof: Elementary, as  $\Gamma^1 - \Gamma^2$  is UV convergent, and hence  $\Gamma_X^1$  and  $\Gamma_X^2$  generate the same counterterm.  $\square$

In particular, we also note that in the above,  $\Gamma_X^1 - \Gamma_X^2$ , when inserted into another graph, produces a result with a bidegree reduced by one unit compared to the insertion of either  $\Gamma_X^1$  or  $\Gamma_X^2$  alone.

This is not yet the desired result, as in our case we have to compare  $\Gamma_{X_1}^1$  with  $\Gamma_{X_2}^2$ , where  $X_1$  is a collection of subgraphs in which all vertex subgraphs are of type  $\Gamma^1$ , and  $X_2$  is the same collection of subgraphs apart from the replacement  $\Gamma^1 \rightarrow \Gamma^2$  for all vertex subgraphs.

Any graph of type  $\Gamma_{X_1}^1$  or  $\Gamma_{X_2}^2$ , which itself can contain subgraphs  $X_i$  of these varying types of vertex corrections plus self-energy subgraphs, can now be expressed in terms of the other. Similarly, this holds for these vertex subgraphs of either type, on the expense of generating extra terms of reduced bidegree

$$\text{bid}(\Gamma_{X_1}^1 - \Gamma_{X_2}^2) < \text{bid}(\Gamma_{X_1}^1) = \text{bid}(\Gamma_{X_2}^2),$$

which involve differences  $\Gamma_{X_i}^1 - \Gamma_{X_i}^2$  for appropriate  $X_i$ . Hence, under the above assumption of monotonic increase of the transcendental weight with the bidegree, we get upon iterating such insertions

**Proposition 2** *The coefficient of the term of maximal transcendental weight is the same for  $\text{res}(\Gamma_{X_1}^1)$  and  $\text{res}(\Gamma_{X_2}^2)$ .*

Here,  $X_1, X_2$  are related, as above.

This explains immediately our results as a look at the functions  $F_{a,b}$ , and hence the corresponding evaluations of our subdivergent graphs, shows that they fulfill the required assumptions of monotonic increase of transcendental weight, which was completely determined from the appearances of the Riemann  $\zeta$ -function in our simple examples. Note that the factorizations into two-point functions and the absence of all other primitive graphs apart from one-loop functions were the two main simplifications which enabled us to satisfy the assumption.

The study to what extent a sensible transcendental weight can be established in general will be a topic of future work. Any sensible answer we will expect to deliver the same permutation invariance of the residue as reported here.

## Acknowledgements

Isabella Bierenbaum acknowledges support by the *Graduiertenkolleg Eichtheorien - Experimentelle Tests und theoretische Grundlagen* at Mainz University.

---

functions or MZVs [19] we do not have to answer here. Also, the attentive reader might have noticed that we set the transcendental weight of the gauge parameter to be zero for the QED results, treating it as an independent variable.

## References

- [1] Christian Bauer, Alexander Frink, Richard Kreckel: *Introduction to the GiNaC Framework for Symbolic Computation within the C++ Programming Language*; to appear in Journal of Symbolic Computation; URL: <http://www.ginac.de> [arXiv:cs-sc/0004015].
- [2] David J. Broadhurst, Dirk Kreimer, *Renormalization automated by Hopf algebra*, J. Symb. Comput. **27** (1999) 581 [arXiv:hep-th/9810087].
- [3] David J. Broadhurst and Dirk Kreimer, *Exact solutions of Dyson-Schwinger equations for iterated one-loop integrals and propagator-coupling duality*, Nucl. Phys. B **600** (2001) 403 [arXiv:hep-th/0012146];  
David J. Broadhurst and Dirk Kreimer, *Combinatoric explosion of renormalization tamed by Hopf algebra: 30-loop Pade-Borel resummation*, Phys. Lett. B **475** (2000) 63 [arXiv:hep-th/9912093].
- [4] Alain Connes and Dirk Kreimer, *Renormalization in quantum field theory and the Riemann-Hilbert problem. II: The beta-function, diffeomorphisms and the renormalization group*, Commun. Math. Phys. **216** (2001) 215 [arXiv:hep-th/0003188];  
Alain Connes and Dirk Kreimer, *Renormalization in quantum field theory and the Riemann-Hilbert problem. I: The Hopf algebra structure of graphs and the main theorem*, Commun. Math. Phys. **210** (2000) 249 [arXiv:hep-th/9912092].
- [5] Dirk Kreimer, *Combinatorics of (perturbative) quantum field theory*, Phys.Repts., in press, arXiv:hep-th/0010059.
- [6] Dirk Kreimer, *Renormalization and knot theory*, J. Knot Theor. Ramifications **6** (1997) 479 [arXiv:q-alg/9607022];  
Robert Delbourgo, David Elliott and David S. McAnally, *Dimensional renormalization in  $\phi^3$  theory: Ladders and rainbows*, Phys. Rev. D **55** (1997) 5230 [arXiv:hep-th/9611150];  
Robert Delbourgo, Alex C. Kalloniatis and George Thompson, *Dimensional renormalization: ladders to rainbows*, Phys. Rev. D **54** (1996) 5373 [arXiv:hep-th/9605107].
- [7] David J. Broadhurst and Dirk Kreimer, *Towards cohomology of renormalization: Bigrading the combinatorial Hopf algebra of rooted trees*, Commun. Math. Phys. **215** (2000) 217 [arXiv:hep-th/0001202].
- [8] Dirk Kreimer, in preparation.
- [9] Dirk Kreimer, *On knots in subdivergent diagrams*, Eur. Phys. J. **C2** (1998) 757 [arXiv:hep-th/9610128].
- [10] Dirk Kreimer and Robert Delbourgo, *Using the Hopf algebra structure of QFT in calculations* Phys. Rev. **D60** (1999) 105025 [arXiv:hep-th/9903249].
- [11] Pedro Pascual and Rolf Tarrach: *QCD: Renormalization for the Practitioner*. Berlin, Springer, 1984. (Lecture Notes in Physics; **194**).
- [12] Available by anonymous FTP from <ftp://ftpthep.physik.uni-mainz.de/pub/bierenbaum/>.

- [13] John C. Collins: *Renormalization*. Cambridge: Cambridge Univ. Press, 1984.
- [14] Dirk Kreimer, *On the Hopf algebra structure of perturbative quantum field theories*, Adv. Theor. Math. Phys. **2** (1998) 303 [arXiv:q-alg/9707029].
- [15] Alain Connes and Dirk Kreimer, *Hopf algebras, renormalization and noncommutative geometry*, Commun. Math. Phys. **199** (1998) 203 [arXiv:hep-th/9808042].
- [16] Dirk Kreimer, *On overlapping divergences*, Commun. Math. Phys. **204** (1999) 669 [arXiv:hep-th/9810022].
- [17] ISO/IEC 14882:1998(E): *Programming languages—C++*; American National Standards Institute, 1998.
- [18] Bruno Haible, Richard Kreckel: *CLN, a Class Library for Numbers*; URL: <http://clisp.cons.org/~haible/packages-cln.html>.
- [19] David J. Broadhurst and Dirk Kreimer, *Knots and numbers in  $\phi^4$  theory to 7 loops and beyond*, Int. J. Mod. Phys. C **6** (1995) 519 [arXiv:hep-ph/9504352].